Chapter 2
Experimental Techniques

Abstract PELDOR or DEER, like most forms of spectroscopy, always involves tradeoffs between sensitivity and resolution. Some tradeoffs are made during the instrumental design of the spectrometers that measure PELDOR spectra, and other tradeoffs are made in the experimental design of the measurements. This chapter considers the instrument design first. It examines the capabilities needed to make PELDOR measurements and then examines the designs of several spectrometers operating at different mw frequencies. This is followed by a discussion of how capabilities of the spectrometer and the operating and measurement parameters affect sensitivity and resolution in PELDOR distance distribution spectra.

2.1 Basic Spectrometer Functions

The PELDOR effect is the change in the ESE signal when pump pulses are applied to the spin system. An ESE spectrometer is necessary to generate and measure the echo signal, but some additional equipment is needed to produce the pump pulses and to apply them to the sample. ESE and PELDOR spectrometers operate in rather narrow mw frequency ranges with $\omega/2\pi$ scattered between 3 and 600 GHz [1–10]. Several different conventions break the microwave (mw) frequency range into a series of bands designated by letters and these bands are used to indicate the approximate operating frequency of spectrometers. A list of some of the more commonly-used designations appear in Table 2.1.

An ESE spectrometer provides much of the core functionality for PELDOR measurements, but requires some additional capabilities. We consider the general functions needed for PELDOR and then look in Sects. 2.2–2.4 at ways several spectrometers implement these requirements.

Table 2.1 Common mw band designations

Band	Frequency $\omega/2\pi$ (GHz)	Wavelength (cm)
L	1–2	15–30
S	2–4	7.5–15
C	4–8	3.75–7.5
X	8–12	2.5–3.75
K_u	12–18	1.67–2.5
K	18–26.5	1.13–1.67
K_a	26.5–40	0.5–1.13
Q	33–50	0.6–0.9
mm	40–300	0.1–0.5
V	40–75	0.4–0.6
W	75–110	0.27–0.4
D	110–170	0.18–0.27

2.1.1 The ESE Core

Several ESE spectrometers have been described in detailed [6, 11–13]. In this section, we focus on the specific features needed for PELDOR measurements. Three different approaches are in use at EPR frequencies through W-band. They are summarized in the simplified block diagrams for a basic PELDOR spectrometer, Fig. 2.1. Each design has, at its core, a standard ESE spectrometer which generates an ESE at ω_A. The performance of this core is one major factor that determines sensitivity, and consequently, the range of distances that can be measured by PELDOR techniques. Therefore, design principles that optimize sensitivity of an ESE spectrometer are also vital for PELDOR measurements.

A low-power mw source on the left side of each block diagram, Fig. 2.1a–c, supplies the mw frequency for the mw pulses and for the signal detector, via a reference arm. The pulse former unit converts the low-power mw output of the source into weak pulses which are amplified by a mw power amplifier and delivered to a mw resonator containing the sample. The ESE goes from the sample in the resonator to the detector where it is converted from a short mw burst into the outline, or envelope, of that burst, known as a video signal. The signal processor block at the right side of the block diagram captures that signal and sends it to a computer where the signals are assembled into a time trace. The pulse programmer block controls and orchestrates all these functions.

2.1.2 MW Source

The mw source for the observe frequency ω_A is usually a voltage-controlled oscillator (VCO), a Gunn diode oscillator with phase-locked loop (PLL) stabilization, or a synthesizer. The ESE is not affected by the phase noise of the mw source to the
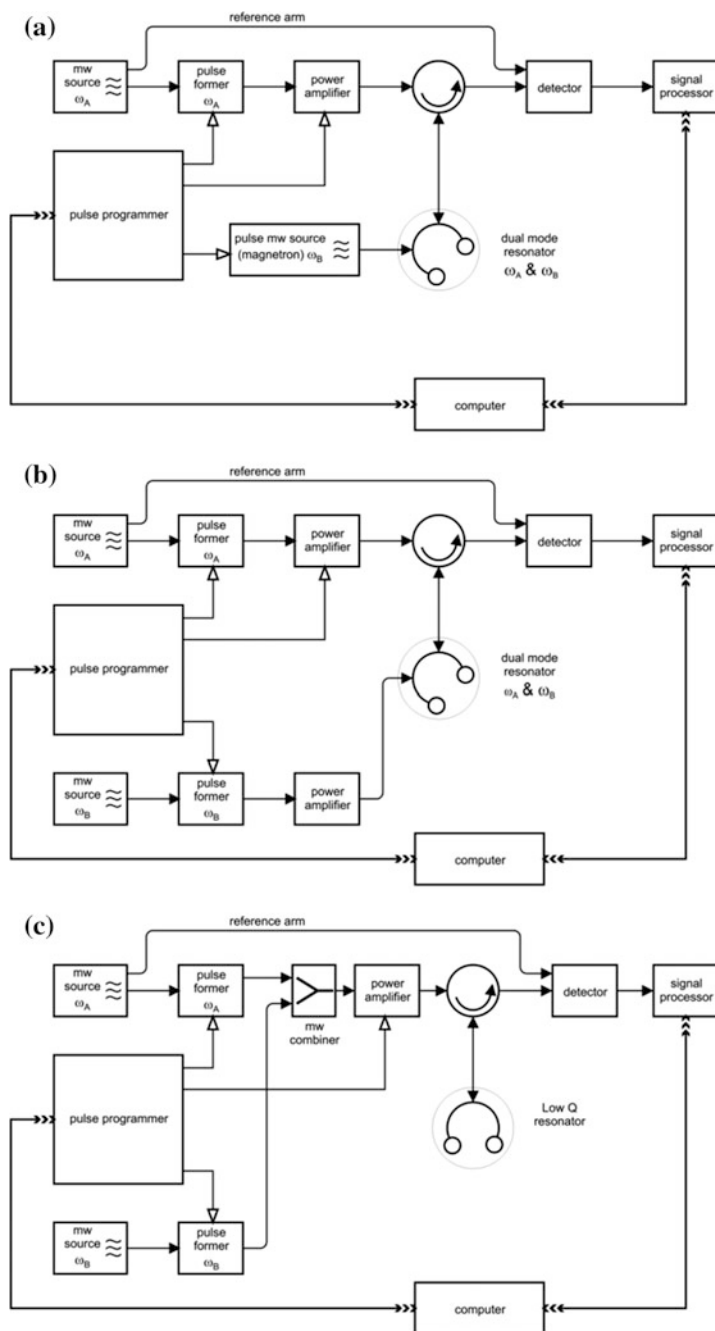
Fig. 2.1 Block diagrams of some X- and Q-band PELDOR spectrometers: **a** bimodal resonator and pulse magnetron as the pump mw source [14]; **b** bimodal resonator and two TWTAs; **c** low Q, overcoupled resonator in most modern spectrometers

extent that the CW EPR signal is, but long-term frequency drift is a problem for signal averaging. There is generally a very large difference between the length of the reference arm and the effective length of the signal-generating arm, particularly when the large propagation delay through a traveling wave tube amplifier (TWTA) is considered. Any difference in effective path length converts frequency drift of the source into a drift in the detected signal phase from the mixer, because the mw mixer is a phase-sensitive detector.

Phase drift during a PELDOR measurement subtly alters the shape of the PELDOR time trace and can impact the distance distribution. But, frequency stability is only one factor in spectrometer phase drift. Two other important factors are resonance-frequency changes in the sample resonator caused by microphonics, sample movement or thermal drift; and voltage regulation of the mw amplifiers, particularly the TWTA accelerating voltage.

Currently, mw oscillators operating at the spectrometer frequency can be used through Q-band. However, a low-frequency source at $\omega/2\pi \approx 6-7$ GHz that is stabilized by a dielectric resonator (DRO) typically is used with subsequent frequency mixing and multiplication for spectrometers operating above Q-band. The DRO serves as the master oscillator, providing low phase and amplitude noise to preserve spectrometer sensitivity.

2.1.3 Pulse Former Unit

The pulse former uses the frequency of the mw source to produce weak mw pulses. The pulse former can be as simple as a mw switch that simply gates the mw output of the source on and off. Most pulse formers also provide control of the amplitude and phase of the pulses, while a few designs produce very complex shaped pulses, chirped pulses or composite pulses. However it is accomplished, it is far easier to form mw pulses at low power and then amplify them than it is to form the pulses from a high power source.

The mw pulses used in PELDOR measurements are fairly short in duration, so that the rising and falling edges can be a significant fraction of the total length, which can impact the pulse excitation spectrum.

2.1.4 Power Amplifier

The mw power amplifier amplifies the low-power mw pulses to the high power levels needed to excite the sample. This amplifier is generally a gated, or pulse, amplifier, meaning that it is in an off state most of the time and is turned on, so that it amplifies, only when needed. A gated amplifier generally consumes much less power than a CW amplifier; power is required only while it is gated on, a few percent of the time. This means it has a smaller, more reliable power supply; is

much cheaper; dissipates much less power; and requires much less cooling. For high-precision measurements where stability is vital, the duty cycle of the power amplifier is best kept constant, to keep the power consumption and temperature of the amplifier constant.

A gated amplifier produces virtually no noise in the off state. An operating amplifier is producing noise. The noise it generates is usually measured in terms of the equivalent thermal noise at the input. So, for example, an amplifier with a 30 dB gain (1000-fold power amplification) and a noise figure of 3 dB (equivalent noise power at the input 2-fold, i.e., 3 dB, higher than thermal noise) would produce noise at its output with 33 dB or 2000 times more power than the thermal noise level at room temperature. The PELDOR signal is often weaker than the room temperature thermal noise level, so noise from the power amplifier must be negligible at the time of the signal. This usually is achievable with amplifiers designed for fast turn-off, however, the amplifier turn off is one contributing factor to the spectrometer dead time.

Gating the amplifier is not a good method to produce short mw pulses. The rise and fall times of the amplifier output are generally much longer than those of a pulse former, and would produce short pulses that have rather triangular or trapezoidal shapes. In addition, there are usually very large phase shifts in the amplified mw output during the rise and fall of the output, resulting in unintended and poorly characterized shaped pulsed that are far from optimal for EPR spectroscopy. If the power amplifier is operated somewhat beyond it linear amplification range in order to obtain the highest power, the pulse shape and phase is subtly altered. Usually the edges become sharper, so pulses are squarer after the power amplifier than at the input.

The power amplifier is usually operated by turning it on; letting it reach a stable operating state; sending one or more mw pulses into it for amplification; and then turning it off. The amplifier may be gated on several times during a single measurement, e.g., once for the first two pulses in a 4pPELDOR measurement, again for the pump pulse, and a final time for the third observe pulse.

2.1.5 Pulse Programmer

A multifunction pulse programmer controls the mw pulses that generate the ESE signal. It controls: the time intervals between the pulses; the pulse width, phase and shape from the pulse formers; and gating of the mw power amplifier. Those factors control when the signal occurs. So the pulse programmer also must control signal acquisition because signal acquisition must be coherently synchronized with signal generation. Signal acquisition involves any gating needed to protect the receiver from damage or overload, and the measurement or digitization of a precise portion of the detected ω_A signal. If signal generation and acquisition use more than one timebase, it is important that they be synchronized and coherent with each other to avoid subtle sources of noise. In PELDOR experiments, the pulse programmer must additionally control the pump pulse at ω_B.

2.1.6 Resonator

The mw pulse sequence at ω_A is fed through a circulator to a resonator containing the sample under investigation. The signal, along with any ringing or reflections from the resonator, comes back to the circulator and is directed to the receiver. The resonator is located inside the computer-controlled magnet, not shown in Fig. 2.1. An iron-core magnet is typical at X- and Q-band and a superconducting cryomagnet at W-band. The resonator supports mw standing waves at ω_A and ω_B. Usually, the sample is placed where the mw electric field is zero, and the mw magnetic field is maximum for both mw frequencies and perpendicular to the field of the surrounding magnet. Resonators are discussed in greater detail in Sect. 2.5.

2.1.7 Detector and Signal Processor

The detector converts the mw burst that is the ESE into a broadband signal centered at zero frequency (homodyne detection), or centered at a lower intermediate frequency ω_{IF} (heterodyne detection). This usually is done by mixing the signal with a mw frequency from the reference arm, ω_A for homodyne detection, or $\omega_A \pm \omega_{IF}$ for heterodyne detection. The resulting signal is then converted into some digital form by the signal processor.

The detector input is usually protected from the power amplifier noise, from the mw pulses themselves, and from ringing of the resonator by a mw limiter or switch that blocks the detector input when appropriate. This protection is needed because too much power can damage or destroy the detector, or can saturate the detector so that its output is distorted. A saturated detector can take quite a long time, microseconds or milliseconds, to recover.

An X-band detector has a low-noise mw preamplifier before the mixer and video amplifiers after the mixer for maximum sensitivity. Detectors at higher mw frequencies are restricted by the limited performance and availability of components and the ESE signal may arrive at the mixer without preamplification.

2.1.8 The PELDOR Arm

In PELDOR experiments, the sample must be exposed to pump mw pulses at ω_B, in the time interval between the observe pulses at ω_A, Figs. 1.1 or 1.2. The pump pulses are often amplified by the same power amplifier as the observe pulses, Fig. 2.2c. Several variations used at X-band are described in Sect. 2.2.

The PELDOR arm contains a mw source for ω_B. It could be derived from ω_A by frequency shifting, but that is not necessary. The PELDOR signal does not depend strongly on the exact frequency or phase of ω_B, and does not require a stable, low-noise mw source. This permits a cheap, non-coherent oscillator to be used for ω_B.

Fig. 2.2 Simplified scheme
of the Bruker BioSpin
intermediate frequency
(IF) PELDOR spectrometer
concept [25, 26]; the
operating frequency band is
defined by an auxiliary
low-power local oscillator
LO, but the pulse sequence
preparation and the signal
detection is carried out at
X-band
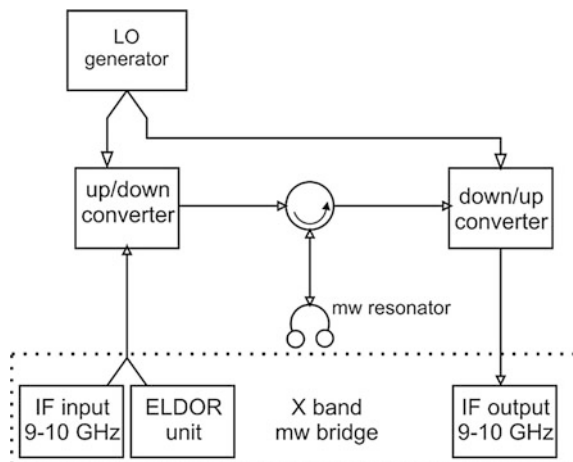
2.2   X- and Q-Band Instruments

Three implementations, at X- and Q-bands, of the basic design just discussed in
Sect. 2.1 are shown in Fig. 2.1. The multiple pulses at ω_A and ω_B are fed into the
resonator two different ways. One design uses a resonator with separate inputs for
each frequency. This requires an independent amplifier for high-power pump pulses
at ω_B, e.g., a magnetron or an independent TWTA, to feed directly into the res-
onator through the "pump" waveguide, Fig. 2.1a, b [15–17].

The other method, Fig. 2.1c, uses only one power amplifier. The low-power
pulses at ω_A and ω_B are combined as a single input to the high-power amplifier and
the output is fed into the resonator. In this case, a single-mode, low-Q resonator is
usually used; while the first method allows use of a single-mode or a bi-modal
resonator. A single-mode resonator is easy to set up and tune, but has poor sen-
sitivity when the frequency difference $\Delta\omega_{AB}$ is large because the resonator Q, and
therefore sensitivity, must be reduced so that both ω_A and ω_B fall within its
bandwidth [15, 18]. High-Q, bimodal resonators achieve good sensitivity [19–22],
but require additional tuning, and additional design care to ensure that the mw
magnetic fields of both modes have strong, uniform overlap at the sample, see
Sect. 2.6.4.

2.2.1   The ICKC Spectrometer

PELDOR spectrometers operating at X-band are currently the most common. The
X-band PELDOR spectrometer based on a coherent pulse EPR spectrometer [14],
Fig. 2.1a, is examined first. This ESE spectrometer was used for many years to
develop and test PELDOR methods at the Voevodsky Institute of Chemical

Kinetics and Combustion (ICKC) in Novosibirsk, Russia. This spectrometer introduced several novel features when it was built, including: independent sources and amplifiers for very intense mw pulses at ω_A and ω_B; and the ability to modulate, or cycle, the phase of the mw observe pulses.

The mw pulses at ω_A can have a power as high as 10 kW with duration $t_p \geq$ 20 ns. These pulses are produced by two-stage amplification of the weak output of a stabilized klystron, which also feeds the reference arm. The weak pulses are amplified to 1 kW by a TWTA. These 1 kW pulses could be used directly as the observe pulses to generate ESE signals or they could be amplified to ~ 10 kW by an injection-locked magnetron which preserves the phase and frequency of the original low-power pulses. This pulse amplification process means that the phase of the high-power mw pulses is controlled at low-power, where it is easily done. This ability to control pulse phase was used to implement phase cycling for the first time in ESE spectroscopy, which reduced the dead time for the ESE signal to ~ 200 ns and eliminated unwanted responses, such as the FID and the resonator ringing [14, 23, 24].

The pulse programmer generates pulses for external synchronization and controls the detector. The pulse duration and the intervals between pulses are discretely controlled with 1 ns increments. The intervals between pulses can extend to 10 ms and can be swept. The programmer also produces a control pulse for the phase shifter, which changes the phase of the first pulse in an ESE sequence. The pulse repetition rate lies between $2 * 10^2$ and 10^4 Hz. The receiver noise factor is 5–6 dB. Digital acquisition of the ESE signal is possible. The magnetic field was controlled by the NMR signal of water protons to an accuracy of 3 ppm.

This ESE spectrometer [14] served as the core for a PELDOR spectrometer. A magnetron operating in a self-excitation mode at a fixed frequency of $\omega_B/2\pi =$ 9400 MHz provided the pump pulses. The magnetron acts as a combined mw source, pulse former and power amplifier, controlled by pulse modulation of its anode voltage. The maximum mw power output of the magnetron is 5 kW with $t_p = 30-40$ ns.

The spectrometer can generate ESE signals from the A or the B spins at the same external magnetic field B_0. To do this, the magnetron gives a pair of pulses at ω_B, forming an ESE signal from B spins at ω_B. That ESE signal is amplified by a mw amplifier, detected by a simple mw diode detector and observed on an oscilloscope. This feature provides a simple, experimental determination of the rotation angle θ of the B spins.

2.2.2 The E580 Spectrometer

Many researchers use the E580 X-band spectrometer from the Bruker BioSpin ELEXYS series for PELDOR measurements, or the earlier ESP 380 model [25–27]. A low-power mw source, or "ELDOR Unit", is added to the main mw

bridge of the basic E580 to provide ω_B, as in Fig. 2.1c. The $\omega_B/2\pi$ of this ELDOR Unit can be set in the range of 9–10 GHz in 100-Hz steps. The $\omega_A/2\pi$ is typically ~ 9.8 GHz, making the maximum difference $\Delta\omega_{AB}/2\pi$ about 800 MHz.

Pulses at ω_A and ω_B are formed by high-speed switches, which provide mw pulses with rise and fall times of 1 ns and a minimum duration of 4–8 ns. Pulses at both ω_A and ω_B are amplified by a single TWTA with a maximum output power of ~ 1 kW. The amplitude, duration, and phase of the ω_A pulses are specified independently from those at ω_B. The amplified pulses are fed into a single-mode, overcoupled dielectric or split-ring resonator. A quadrature mixer preceded by a low-noise preamplifier detects the signals.

The fact that pulses at both frequencies are formed independently, but amplified by the same TWTA, is an important difference between the E580 and the spectrometer developed by the ICKC [14]. This has meant that only single-mode, broadband resonators are used with the E580, while the ICKC spectrometer [14] uses a bimodal rectangular resonator with two waveguide inputs: one for pulses at ω_A from the TWTA, and the other for pulses at ω_B from the magnetron.

2.3   High-Frequency Instruments

PELDOR spectrometers at frequencies above X-band face practical and technical limitations. In particular, bimodal resonator design becomes increasingly difficult at high frequencies. This restricts the frequency difference $\Delta\omega_{AB}$ to the resonator bandwidth.

EPR spectra of unoriented paramagnetic centers become considerably broader at frequencies above X-band due to g-factor anisotropy. Consequently, the PELDOR modulation is considerably weaker for comparable pump pulses at frequencies beyond X-band, because the degree of excitation of the spectrum p_B decreases. However, these high-frequency limitations greatly improve orientation selection.

2.3.1   The IF Approach

The X-band E580 spectrometer of Bruker BioSpin [25, 26] can be modified for use in the L-, S-, Q-, and W bands for CW and pulse EPR, including PELDOR [26, 27]. These modifications use the Intermediate Frequency (IF) concept for operating frequencies outside the X-band, Fig. 2.2. The most significant advantage of this approach is that proven X-band technology is used for excitation and detection regardless of the operating EPR frequency.

A pulsed spectrometer operating at both the X- and Ku-bands was developed at Cornell University mainly for double quantum coherence (DQC) spectroscopy [28]. This spectrometer uses pulses with an excitation bandwidth of ~ 70 G or $\sim 2\pi *$

200 MHz and can excite the whole EPR spectrum of nitroxyl labels for DQC experiments.

A homodyne double-channel X-band bridge forms pulses with a duration of 3–5 ns at four fixed phases with a minimum separation in time of 5 ns. This bridge applies the IF concept to operate at Ku band, $\sim 2\pi*17$ GHz. A pump pulse module allows PELDOR measurements at both bands. The frequency difference $\Delta\omega_{AB}/2\pi$ can be selected in the range of 0–700 MHz.

2.3.2   W-Band Instruments

A homodyne W-band spectrometer [29] similar to Fig. 2.1c or Fig. 6 of [30], has two independent mw sources based on frequency multiplication. The tunable source consists of an $\sim 2\pi*7.3$-GHz master oscillator and a $\times 13$ frequency multiplier, giving $\omega_B/2\pi$ in the range of 94.9 $\pm$ 1.3 GHz with steps of 13 kHz. A similar source has a fixed frequency for $\omega_A/2\pi = 94.9$ GHz. The pulses are formed by independent pulse formers with high-frequency p–i–n diode switches and they are combined as the input to a solid-state mw power amplifier with up to 1 W output power. The pulse power at the input of the TE_{100} cylindrical resonator is estimated to be 300–350 mW [29]. With a loaded Q-value, $Q_L \sim 1000$, the π pulse has a duration $t_p \sim 26$ ns. The spectrometer dead time is ~ 50 ns with the resonator at room temperature and ~ 150 ns at low temperature because conductivity of the resonator walls and, therefore, the Q-value, increase.

A top-of-the-line W-band spectrometer, Fig. 2.3, was developed at the Free University of Berlin [31–33]. The cryomagnet has a 114 mm diameter warm bore, to accommodate a helium cryostat with a useful diameter of ~ 90 mm. Field scans of up to 1000 G are performed by auxiliary superconducting sweep coils. The mw bridge is based on a heterodyne circuit with an intermediate frequency of $2\pi*4$ GHz. Three DRO master oscillators with similar frequencies of $\sim 2\pi*7$ GHz are available to help track the natural frequency of the resonator.

After multiplication by $\times 13$, ~ 10 mW of the mw power at $\omega_A/2\pi = 95$ GHz is used to produce the local oscillator $\omega_{LO}/2\pi = 99$ GHz for the detector; the rest passes through a system of pulse-forming switches and phase shifters to the input of an IMPATT diode amplifier with ~ 300 mW output power, and then through an attenuator and circulator to a cylindrical TE_{011} or Fabry–Perot resonator.

The EPR signals pass back through the circulator and a p–i–n switch which protects the receiver from high-power reflected mw pulses. The signal is mixed down to $\omega_{IF}/2\pi = 4$ GHz; amplified by a LNA; converted to a video signal by the quadrature detector; and the components of the EPR signal are fed into the signal processor.

The dead time of the spectrometer in pulse mode is ~ 20 ns, and the noise figure of the mw receiver is 11 dB or better. PELDOR results from this spectrometer on the geometry and distances in photosynthetic reactive centers are discussed in Sect. 7.2.2.
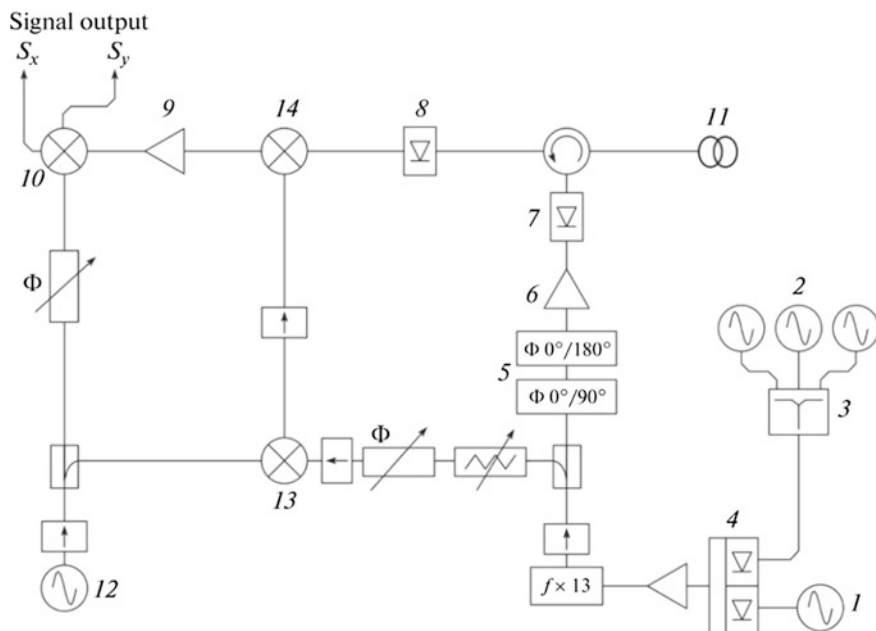
Fig. 2.3 Block diagram of a pulsed 95 GHz heterodyne EPR spectrometer [30]: *1* oscillator at $\omega/2\pi = 7.3 \pm 0.023$ GHz; *2* oscillators at $7.3 + 0.23$, 7.3, and $7.3-0.23$ GHz; *3* power combiner; *4*, *7* fast p–i–n switches; *5* fast phase modulators; *6* avalanche-transit diode power amplifier; *8* protective fast p–i–n diode switch; *9* a 4 GHz LNA amplifier; *10* mixer–quadrature detector; *11* TE011 resonator; *12* a 4 GHz oscillator; *13* mixer to generate the local oscillator $\omega_{LO}/2\pi = 4 + 95 = 99$ GHz; and *14* mixer to shift the signal to $\omega_{IF}/2\pi = 99 - 95 = 4$ GHz

2.3.3 180 GHz PELDOR

Several laboratories have designed PELDOR spectrometers operating above W-band. One is a heterodyne pulse EPR spectrometer operating at $\omega_A/2\pi \approx 180$ GHz, Fig. 2.4 [34–36]. The spectrometer generates the mw pulse sequence at $\sim 2\pi*45$ GHz and then doubles the frequency twice to obtain $\omega_A/2\pi \approx \omega_B/2\pi \approx 180$ GHz.

Pulses of ~ 100 ns duration are formed by switches in two independent channels and combined by a magic-T coupler. The mw pulse sequence is frequency doubled, amplified, doubled again. Waveguide circulators are not available at this band, so a quasi-optical circulator delivers ~ 20 mW to a cylindrical resonator with an inner diameter of 2.2 mm via low-loss corrugated oversized waveguide.

An elliptical mirror focuses the ESE signal from the resonator into the receiver through a conical waveguide taper. The cryogenic magnet of the spectrometer creates a static magnetic field of up to 7.0 T with a sweep range of 1.5 kg. This spectrometer was used to investigate the orientation selection in pairs of tyrosine radicals in proteins [37, 38].
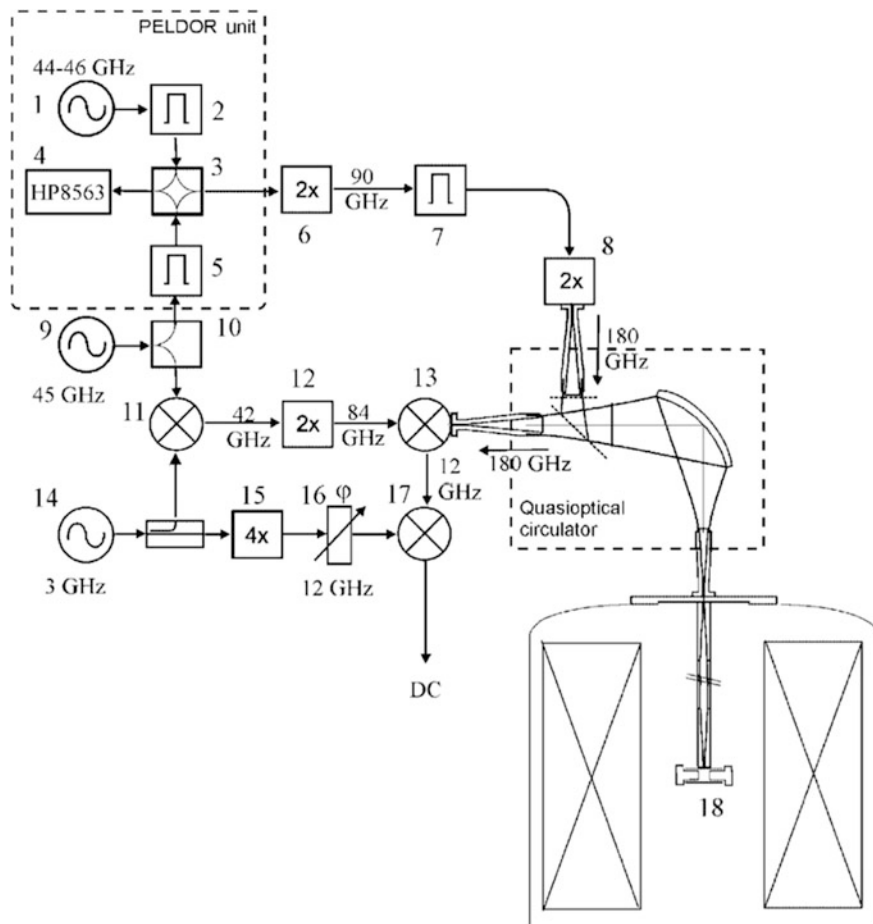
Fig. 2.4 Block diagram of a 180 GHz pulse EPR/ELDOR spectrometer: *1* variable frequency oscillator; *2*, *5*, *7* fast switches; *3* magic-T; *4* spectrum analyzer; *6*, *8*, *12* frequency doublers; *9*, *14* oscillators; *10* power divider; *11*, *13*, *17* mixers; *15* frequency multiplier; *16* phase shifter; *18* resonator; 45 GHz amplifiers are omitted for clarity. Reproduced from Hertel et al. [35], with permission of John Wiley and Sons, copyright 2005

2.3.4   263 GHz PELDOR

The record high $\omega_A/2\pi \approx 263$ GHz quasi-optical commercial spectrometer was designed by Bruker BioSpin. The BRUKER E780 instrument [10, 39] performs CW and pulse EPR experiments at magnetic fields close to 9.4 T. The mw bridge is based on a heterodyne IF design consisting of two units: an X-band transmitter/ receiver and the 263 GHz quasi-optical front-end. This minimizes the number of millimeter-wave components by performing the crucial mw generation and signal detection at X-band. The X-band transmitter includes two mw sources.

A TE_{011} single-mode resonator is coupled to the quasi-optical front-end via a mode converter and corrugated waveguide, which substantially reduces mw losses to below 1 dB. The resonator Q-value can reach 1000 and, with the mw power of 15 mW at the resonator, the optimal $\pi/2$ pulse duration is 50–55 ns. Since the size of the resonator scales with mw wavelength, $\lambda \sim 1$ mm, the sample tube has outer and inner diameters as small as 0.33 and 0.2 mm, respectively, with a sample volume ~ 30 nL for a 1 mm long sample.

Impressive spectral and orientation resolution is achieved. Specifically, at $B_0 \sim 9.6$ T, the g-factor resolution is 30-fold better than at X-band and ~ 3 better than W-band. This gives much higher orientation selection for PELDOR.

However, PELDOR experiments at 263 GHz are more difficult to implement and execute [10]. The limited power and increased mw losses require long pulses, giving weaker EPR signals, while g-anisotropy produces broader EPR spectra. One expects weaker modulation but better orientation selection than at lower frequencies. The high absolute sensitivity of the HF-EPR spectrometer allows PELDOR measurements on samples with limited volumes, particularly promising for rare biological/biochemical materials.

2.4 B_0-Jump PELDOR

The PELDOR spectrometers described above use two mw sources for ω_A and ω_B. An alternative approach is to rapidly change the magnetic field from $B_0 = \omega_A/2\pi\gamma$, by ΔB_0, corresponding to a pump frequency $\omega_B = \gamma(B_0 + \Delta B_0)$. PELDOR or ESE experiments based on this technique were proposed and conducted to measure spin–lattice relaxation, spectral diffusion [40], and transfer of saturation in EPR spectra, and for studying slow molecular motions [41–43].

The PELDOR method with B_0 jump was used to determine distances between spins in biradical **3-1** and in a related biradical [44]. The three-pulse stimulated ESE, Fig. 2.5, enabled detection of the signal. A magnetic field jump equivalent to the pump frequency $(\Delta\omega_{AB} = \gamma\Delta B)$ was applied between the second and third pulses of the three pulse stimulated ESE sequence, Fig. 2.5a or a field sweep provided very broad pump excitation, Fig. 2.5b. The stimulated ESE was measured as a function of the delay τ between the first and second pulses.

A Bruker BioSpin ESP-380 pulse spectrometer was used with a rectangular H_{102} resonator modified with walls of thin 25 μm foil of nonmagnetic stainless steel that was "semi-transparent" to the magnetic field pulse [44]. The magnetic field pulse was produced by low-inductance coils replacing the modulation coils. The low mw conductivity of the walls gave the low Q required for PELDOR experiments. The pulse current source creating the field jump contains corrective RC-circuits to produce the flattest possible field pulse with minimum rise and fall times. The shift of the EPR line in the ESE-detected spectrum was used to determine that the rise and fall times of the magnetic field pulse were under 1 μs. The maximum magnetic
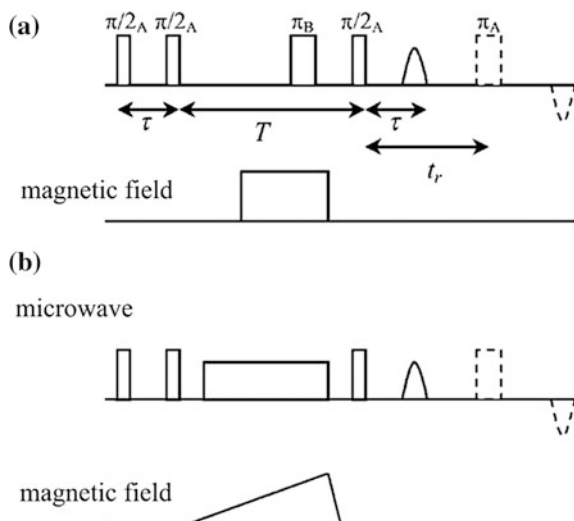
Fig. 2.5 Pulse sequences for field-step ELDOR: the three-pulse stimulated ESE sequence $\pi/2_A - \tau - \pi/2_A - T - \pi/2_A - \tau - echo$ with the pump pulse π_B during the field jump. **a** Pumping with fixed magnetic field jump; **b** scanning pumping; to overcome the dead time problem, the ESE may be refocused by an additional π_A pulse (*dashed line*). Reproduced from Kulik et al. [44] with permission of Elsevier Limited, copyright 2002

field pulse amplitude was ± 170 G, and the pulse duration could be set from $1.0\,\mu s$ to $1.0\,s$ [44].

A similar setup for magnetic field jump PELDOR experiments has been used at W-band [32]. The advantage of field jumps over the double-frequency PELDOR method is quite clear at W-band: it permits use of a high-Q resonator to obtain the highest-possible sensitivity. PELDOR using a magnetic field jump seems very promising; it does not require a second mw source for the pump pulse, which becomes expensive at higher frequencies. The pulsed field version of PELDOR shares all the advantages of existing single-frequency EPR methods.

2.5 Resonators: Construction, Q, and Dead Time

The resonator is located inside the EPR magnet—an iron-core magnet for X- and Q-band, or a superconducting cryomagnet for W-band. The resonator has several mw standing waves or modes. Usually, the frequencies of only one mode, for a single-mode resonator, or two modes, for a bimodal resonator, fall in the frequency range of the spectrometer. Ideally, the sample is placed where the mw electric field is zero and the mw magnetic field is maximum and perpendicular to the field of the surrounding magnet.

In PELDOR experiments, the sample must be exposed to pump pulses at ω_B, in the time interval between the pulses at frequency ω_A, Figs. 1.1 and 1.2. Two ways are used to feed the multiple pulses at ω_A and ω_B into the resonator depending on whether it is a single-mode or a bimodal resonator, Sect. 2.2.

A single-mode, low-Q resonator is relatively easy to design and build. It has only one active mode, so the bandwidth must be large to support the mw fields at both ω_A and ω_B. Single-mode resonators usually have only one input and are said to operate in reflection because the signal travels in the opposite direction from the resonator from the observe pulses. However, single mode resonators with two inputs/outputs have been used and operate in transmission. Because the same resonator mode is used for both frequencies, the mw magnetic fields of both frequencies have excellent spatial overlap, which is important for PELDOR. A single-mode resonator is easy to tune and operate, but has poor sensitivity when the frequency difference $\Delta\omega_{AB}$ is large because the resonator Q, and therefore sensitivity, must be reduced so that both ω_A and ω_B fall within the resonator bandwidth.

Bimodal resonators achieve good sensitivity by using separate high-Q modes for ω_A and ω_B [3, 19–22], but introduce several difficulties. Bimodal resonators suitable for PELDOR are difficult to design because: the two modes must be tunable to the desired ω_A and ω_B; the mw magnetic field maximum of each mode must uniformly overlap each other and the sample; and mw magnetic fields of each mode must be perpendicular to the field of the EPR magnet. In addition, an input specific for each mode is usually desired. It is possible to excite both modes from a single input, but requires a method of adjusting the coupling to each mode. At high mw frequencies, bimodal resonators require very exacting mechanical tolerances and adjustments, making them difficult to construct and use. New approaches to bimodal resonator design do show promise [22].

2.5.1   Resonator Properties

The resonator for PELDOR experiments has two conflicting requirements. First, it must create large mw B_1 fields at the sample to excite a large portion of the EPR spectrum. For instance, to flip spins at $g = 2.0$ by a π turning angle, a 10-ns duration pulse must have a mw field amplitude of $B_1 \sim 10$ G. Second, the resonator must excite the sample at two frequencies ω_A and ω_B. These two requirements are difficult to satisfy simultaneously.

In CW EPR spectrometers, the B_1 in a resonator depends on its Q_{Loaded} and the mw input power P:

$$B_1 = \delta(Q_{Loaded}P)^{1/2}$$
$$Q_{Loaded} = \frac{\omega_0}{\Delta\omega} \tag{2.1}$$

where δ is a parameter depending on the resonator design and sample position; ω_0 and $\Delta\omega$ are the resonant frequency and the resonator bandwidth, respectively.

The mw power incident on the resonator input is usually limited in a PELDOR spectrometer; at X-band, to ~ 1 kW. The simplest method to increase B_1 is to increase the resonator Q, as it is usually done in CW EPR spectroscopy; but this is unacceptable for pulse EPR spectroscopy, since a high Q factor increases the dead time due to resonator ringing and distorts the mw pulse shape. To avoid distorting short, rectangular pulses, the band width of the resonator must satisfy the condition [4]

$$\frac{\Delta\omega}{2\pi} \geq \frac{0.57}{t_p} \tag{2.2}$$

where t_p is the pulse duration, limiting the Q factor to

$$Q_{Opt} \leq 1.75 t_p \frac{\omega_0}{2\pi}. \tag{2.3}$$

This means, at X-band, that the Q factor for undistorted 10 ns rectangular pulses is $Q_{Opt} \leq 175$.

The dead time is the interval after a pulse during which the signal cannot be measured. Many factors contribute to the dead time including: unwanted signals, such as the FID; mismatches and reflections in the mw circuit; noise from power amplifiers; recovery of amplifiers from overload; and the "ringing" of the resonator after the last mw pulse. The resonator ringing must decay to roughly the level of the noise power, which takes a time t_R, illustrated in Fig. 2.6.

The dead time is an important consideration in ESE spectroscopy because the ESE intensity at small τ is important. This is not the case in 3p- and 4pPELDOR measurements which typically use fairly large values of $\tau > t_R$, with

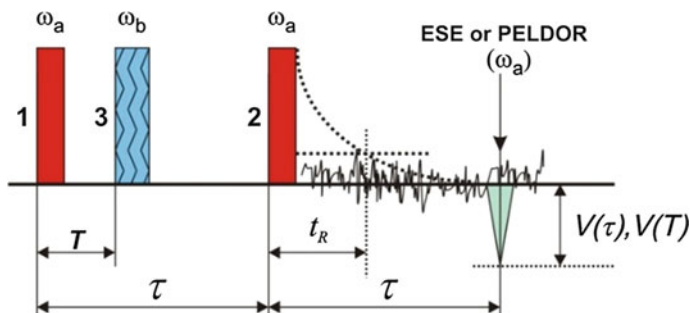$$t_R = \frac{Q}{2\omega_0} \ln\left(\frac{P_0}{P_n}\right) \tag{2.4}$$

Fig. 2.6 Dead time or ringdown time in 3pPELDOR

where P_0 is the mw pulse power and $P_n = kT\omega_0/2Q$ is the noise power. Estimates for $P_0 = 1\,\text{kW}$, $Q = 500$, $T = 300\,\text{K}$, and $\omega_0/2\pi = 9\,\text{GHz}$, give $t_R = 120\,\text{ns}$. A detailed analysis was presented in [11, 32, 45].

If it is necessary to reduce t_R, Eq. (2.4) shows that low-Q resonators must be used. However, this reduces sensitivity proportional to $Q^{1/2}$. A number of methods to reduce the dead time from ringing are used in pulse EPR spectroscopy, including: mw delay lines [38, 46, 47], mw pulse phase cycling [14], remote or refocused ESE [48, 49], bimodal resonators [15–17], loop-gap resonators [50], and detection of longitudinal magnetization [51].

2.5.2   Single-Mode Resonators

The Q-value must be low if a single-mode resonator is used for PELDOR experiments:

$$Q \le \frac{\omega_0}{\Delta\omega_{AB}}. \tag{2.5}$$

With nitroxyl labels and organic radicals, $\Delta\omega_{AB}/2\pi$ can be $\ge$ 80–100 MHz at X-band, limiting Q to 100–130. For single-mode resonators, the competing need for a high B_1 and a low Q-value can be satisfied only by replacing standard cavity resonators with special resonant structures.

There are several methods to achieve the B_1 required in a single-mode resonator. One is to use semi-lumped structures in which the electric and magnetic mw fields are spatially separated, e.g., resonant helices [52], slotted-tube resonators [53], loop-gap resonators [50, 54], and split-ring resonators [15]. Such resonators have a much smaller volume, which increases B_1 and largely compensates for the loss of sensitivity from the low Q-value. The pioneering CW electron double resonance work used a helical resonator [55] and a rectangular bimodal resonant cavity [19].

The low-Q dielectric resonator ER 4118X-MD-5 from Bruker BioSpin [56] is widely used at X-band. Its dielectric resonator is an alumina tube made from a single crystal of Al_2O_3. It has good sensitivity, provides reasonable B_1 at moderate mw power, and its resonant frequency changes only a few MHz with temperature. But, it is extremely difficult to make alumina that is absolutely free of Cr(III) ions and even a trace amount produces rather strong signals in EPR spectra. These impurity signals are temperature dependent and can complicate data analysis and interpretation of weak samples. ESE signals from the impurity Cr(III) signal is generally seen only near 4 K for very short values of τ and is not a common problem for PELDOR measurements of nitroxyl labels and other organic radicals. Replacement of the standard alumina tube by a bismuth germinate, $Bi_4(GeO_4)_3$ or BGO, tube reduces the CW EPR impurity signals and the resonant frequency changes very little with temperature [57].

A cylindrical TE_{011} mode dielectric resonator at K_a-band with $\omega_A/2\pi = 33{-}34$ GHz was constructed for PELDOR measurements at cryogenic temperatures [18]. The estimated Q_{Loaded} was about 180, pulse duration was 10 ns for pump and 17 ns for observe pulses at $\Delta\omega_{AB}/2\pi \sim 180$ MHz.

A very effective method of increasing the bandwidth of the resonator and lowering the resonator Q-value is to increase its coupling to the waveguide or transmission line, i.e., overcoupling, so $\beta > 1$. Adjustment of the coupling [25, 58] changes Q_{Loaded}, $\Delta\omega$, and B_1. Resonance curves for dielectric resonators and split-ring resonators used by Bruker Biospin in PELDOR experiments are presented in [15]. For these resonators at $\Delta\omega_{AB}/2\pi = 500$ (dielectric resonator) and 700 MHz (split-ring), field strength $\gamma B_1/2\pi$ may be as high as 90 and 60 MHz, depending on the extent of overcoupling.

2.5.3 Bimodal Resonators

Crossed bimodal cavity resonators have found wide application in CW double resonance spectroscopy [59]. Bimodal resonators with $\omega_A = \omega_B$ but having mutually-orthogonal mw B_1 fields at the sample are used in pulse EPR spectroscopy to "uncouple" signal excitation from detection and reduce spectrometer dead time. The isolation between modes may be as high as 70–80 dB. The mw pulses in one resonator mode that excite the ESE signal are substantially attenuated in the other mode for detection. As a result, devices to protect the detector are no longer needed, reducing the dead time for an ESE signal to 30 ns. Bimodal resonators can be tuned for PELDOR with one mode resonant at ω_A and the other at ω_B, giving good sensitivity and large B_1 for $\Delta\omega_{AB}/2\pi = 700$ MHz or more.

The crossed bimodal cavity resonator used in PELDOR studies with the ICKC spectrometer is similar in design to the resonator proposed for CW double resonance experiments [19]. Both modes of the resonator are tuned by introducing quartz or Teflon rods in the appropriate volume. The coupling between the modes is -20 to -30 dB at $\omega_A/2\pi = 9.4$ GHz with $Q_A = 220$ and $Q_B = 150$. The $\Delta\omega_{AB}/2\pi$ may be set as large as 150 MHz.

At W-band, a double-cylindrical cavity was designed with two mw modes TE_{011} and TE_{012} rather close in frequency [22]. The sample is placed along the axis of the collinear cylinders. This is a novel arrangement for bimodal resonators for PELDOR because the mw B_1 fields of both modes are coaxial, not crossed. The quality factor is 4400 for the TE_{012} mode and 2900 for the TE_{011} mode. The mw B_1 fields measured by nutation at only 400 mW of mw power are 3.1 G and 2.9 G, respectively. The frequency difference $\Delta\omega_{AB}/2\pi$ between the TE_{012} and TE_{011} modes may be adjusted from ~ 80 to ~ 660 MHz for orientation selection experiments.

2.6   Performance Considerations

2.6.1   Sensitivity

The sensitivity in PELDOR experiments, in terms of the minimum number of particles detected, is governed by the sensitivity of the base ESE spectrometer. The initial amplitude of the PELDOR signal at a fixed τ corresponds to the ESE signal amplitude. Calculations of ESE spectrometer sensitivities have been made many times, e.g., see [1, 4, 11, 59]. One way to express the sensitivity is as the signal-to-noise ratio relative to the unavoidable noise from random thermal fluctuations in the spectrometer. For excitation of the full spectrum, the signal-to-noise ratio, S/N, for pulse EPR spectrometers depends on the operating frequency as [17, 31]:

$$(S/N)_0 \propto \left[\frac{Q_0}{V_0 F \Delta kT} \right]^{1/2} \frac{\omega_0^n}{kT} \qquad (2.6)$$

where V_0 is the effective resonator volume, F is the noise figure of the receiver, Δ is the receiver bandwidth, k is the Boltzmann constant, and T is temperature. The exponent n depends on specific experimental conditions and can even change sign: $7/2 \leq n \leq -3/2$. For instance, for a small sample with a constant number of spins, n = 3/2 [60].

The minimal detectable number of spins for an "ideal" ESE spectrometer is [4]:

$$N_{min} = \frac{4\gamma kT}{g^2 \beta^2 T_2^* \omega_0^2} \sqrt{\frac{2kT_B V_0 T_1}{0.79 \pi t_R}} \qquad (2.7)$$

where g is the electron g-factor, β the Bohr magneton, t_R the measurement time, and T_1, T_2^* are relaxation times. This formula assumes that the two pulses can be placed close enough in time that ESE decay is negligible.

As a rule, sensitivity increases with frequency. For example, under similar experimental conditions, sensitivity at X-band appeared to be 30–40 times higher than at S-band [61]. The sensitivity of Q-band spectrometers was $10-10^3$ times higher than that of X-band spectrometers, depending on the experimental conditions [62]. A comprehensive analysis of ESE spectrometer sensitivity was reported in [17].

Sensitivity can be increased by signal averaging. The efficiency depends on the signal detection method used: coherent, i.e., phase-sensitive, or incoherent. For coherent detection, sensitivity increases with the square root of the number of averages $\sqrt{N}$, while for incoherent detection, sensitivity increases more slowly as $\sqrt[4]{N}$ [4]. The optimum pulse repetition rate for signal averaging is [4]

$$\upsilon_{opt} = \frac{0.8}{T_1} \qquad (2.8)$$

but only if the rate does not vary. Pauses or fluctuations in the pulse rate, e.g., for data transfers or computer overhead, can produce large spikes known as 'T_1' noise that does not average efficiently.

The sensitivity of an ideal coherent X-band ESE spectrometer is about $10^{10} - 10^{11}$ spins [4], provided that the spectrum is fully excited and the relaxation times were $T_1 = T_2 = 10^{-6}$s. This corresponds to the sensitivity of state-of-the-art CW EPR spectrometers.

The actual sensitivity of a pulse spectrometer is considerably worse for several reasons. The first is non-optimal design of the resonator. Short duration pump pulses and ESE signals require large resonator bandwidth and a low Q-value, leading to a small signal and a small S/N ratio. The second reason is non-optimal repetition rate for the observe pulses, and, finally, incomplete excitation caused by large spectral width or inhomogeneity of B_1 over the sample. The influence of all these factors was thoroughly discussed in [1, 4]. As a rule, the sensitivity of pulse spectrometers is 10–100 times lower than the sensitivity of CW instruments. PELDOR measurements can typically be made with about 100 μM spin label concentration in 50 μL of sample by commercial X-band spectrometers.

A characteristic of PELDOR experiments is that they are performed with a fixed time τ_0 between the ω_A pulses that produce the ESE signal. The τ_0 is generally not extremely short, since this would limit the time interval T and truncate the PELDOR time trace, causing a loss of distance information. Consequently, considerable phase relaxation and decay of the ESE signal occur. The PELDOR signal intensity (measurement sensitivity) decreases at large τ_0 by phase relaxation characterized by a time T_f, so that:

$$S/N \sim (S/N)_0 \exp\left(-\left(\frac{\tau_0}{T_f}\right)^n\right) \tag{2.9}$$

with n between 1 and 2 [4, 63]. The PELDOR information is only a small fraction of the ESE signal and is proportional to p_B, further decreasing the PELDOR S/N ratio.

The sensitivity in PELDOR experiments is several times lower than in ordinary pulse EPR experiments. Experience suggests that a sample of spin-labeled protein and other biopolymer should contain $\geq 10^{12}$ molecules for a reliable distance distribution measurement.

However, there is considerable opportunity to improve the experimental PELDOR sensitivity by: deuterating the matrix and protein [64, 65], varying times T and τ during the measurement [66], measuring at higher mw frequencies [67–69], exploiting light-induced electron spin polarization [70, 71], using alternative pulse sequences [13, 42], improving the spin labels [72–76], employing bimodal resonators [22, 77], stitching together measurements from complementary 3p and 4p pulse sequences [78], and optimizing the tuning of pump and observe pulses [79].

2.6.2   Signal Processing Improvements

Sensitivity improvements are not limited just to increasing the signal. Removal of noise from the measurement also increases the *S/N* ratio. This is seen with phase cycling to remove resonator ringing and FIDs from the PELDOR time traces. Recently, a promising technique for increasing PELDOR sensitivity using a wavelet transform was demonstrated [80–82]. This basically removes noise from the time trace that does not have the characteristics of a PELDOR signal. Reduction of signal averaging times for time-domain signals by as much as two orders of magnitude was shown, while retaining the fidelity of the underlying signals. Excellent signal recovery was possible when the initial noisy signal has an $S/N \gtrsim 3$. The two order of magnitude reduction in signal averaging reported corresponds to a ten-fold sensitivity increase.

2.6.3   PELDOR Distance Range

The range of distances r that can be measured from oscillations of the PELDOR signal is limited by the range of times T in the PELDOR time trace. Roughly, a half-cycle of an oscillation is needed to determine its frequency accurately. The PELDOR signal oscillations occur at the dipolar frequency $\omega_D = \gamma^2 \hbar / r^3$. Thus, the minimum dipole frequency, or maximum distance r_{max}, that can be measured, is limited by the maximum time interval T_{max} in the PELDOR time trace. Because the PELDOR signal is measured from a two-pulse ESE, T_{max} must be less than the interval τ_0 between detection pulses. These considerations set a distance limit of

$$r_{max} \approx \left[\frac{\gamma^2 \hbar}{\pi} \tau_0 \right]^{1/3}. \tag{2.10}$$

The two-pulse ESE signal decay sets a practical limit on τ_0. The ESE intensity decreases as τ increases in a process known as phase relaxation, characterized by a time constant T_f. Phase relaxation has a complex dependence on the concentration of electron and nuclear spins, temperature, molecular motion and other properties of the spin system. In PELDOR experiments, the high concentrations of protons, e.g., in proteins, organics or frozen aqueous solutions, commonly set an upper limit on T_f. Spin diffusion among the proton spins drives spectral diffusion of the electron spins, and phase relaxation, even at temperatures below 4 K [4, 63]. Proton spin diffusion causes the ESE to relax at large τ roughly as $\exp\left[-\left(\tau/T_f\right)^2\right]$, with $T_f \sim 2 - 5\,\mu s$ for typical organic or aqueous matrices. The value of $\tau_0 \sim 5\,\mu s$ gives a reasonable benchmark of $r_{max} \sim 8$ nm. Deuteration of the matrix can increase T_f, making measurements at $\tau_0 > 50\,\mu s$ feasible [64, 65], for $r_{max} \sim 16$ nm.

The classic PELDOR modulation, Eq. 1.10, was derived for uniform excitation of each Pake doublet, which are roughly $2\omega_D$ wide. Thus, uniform excitation requires $\gamma B_1 > 2\omega_D$ for both the pump and the observe pulses, or $\pi > 2\omega_D t_\pi$ for both ω_A and ω_B where t_π is the duration of π pulses. This sets a minimum distance of

$$r_{min} = \left[2\frac{\gamma^2\hbar}{\pi}t_\pi\right]^{1/3} \tag{2.11}$$

for $t_\pi \sim 30$ ns, $r_{min} \sim 1.2$ nm. Small exchange interactions between radicals becomes comparable to ω_D at this distance, see Sect. 3.4, complicating measurement of the distance.

These rough estimates indicate that the range of distances measurable from oscillations of the PELDOR time trace is 1.2–8.0 nm. In practice, the range seems to be more like $r_{min} \geq 1.6$ nm and $r_{max} \leq 8$ nm, although this range can be enlarged in some situations. The distance distribution $F(r)$ between spins can be determined reliably over this entire range.

2.6.4 Measurement of B_1

In pulse EPR spectroscopy, it is important that the spectrometer be adjusted so that mw pulses turn the spin magnetization through specified angles θ. This is done by adjusting the amplitude B_1 or duration t_p of the mw pulses. For example, in PELDOR experiments, the pump pulse at ω_B usually has a π turning angle and the observe pulses at ω_A have $\pi/2$ and π turning angles.

The B_1 must be determined not at its maximum in the resonator, but at the site of the sample under investigation. The easiest way to do this is to measure the nutation signal, or Tory oscillations, for a sample with a narrow EPR line [15, 83, 84]. The full spectral line must be excited and the sample must have a long phase relaxation time.

Coal is a convenient and frequently-used solid sample for determining B_1, but the EPR characteristics of coal vary with its source and its exposure to air. Solutions of stable radicals with EPR lines that are narrow in comparison with B_1, e.g., Fremy's salt **5-2**, are also used [83]. In these nutation experiments, the signal amplitude is modulated at the frequency, $\omega_1 = \gamma B_1$, permitting direct measurement of B_1.

Another convenient approach allows B_1 to be determined using the PELDOR sample in the resonator. This method is applicable both for narrow and broad EPR spectra. The shape of the ESE from two, equal-width mw pulses is recorded while varying the amplitude of the pulses at the peak of the EPR spectrum. The ESE signal, for incoherent or 'power' detection, is a symmetric double peak with a dip at

the center when $\theta = \pi$ for either full or partial excitation of the spectrum [1, 4, 30]. With modern spectrometers, the in-phase signal is antisymmetric with positive and negative lobes of equal amplitude and shape.

Once θ is known for a specific set of conditions, it may be adjusted to any desired value using a calibrated mw attenuator between the power amplifier and the resonator to set the mw power going into the resonator. This method is far more accurate than adjusting the pulse width, because the nominal pulse width is often different from the actual width, and because the rise and fall times of the mw field in the resonator are not negligible.

The value of B_1 depends on the mw pulse frequency relative to resonator frequency. With a single mode resonator, at least one mw frequency differs from that of the resonator in a PELDOR experiment, Fig. 2.7a, and its B_1 is reduced. This off-resonant reduction is in addition to the B_1 reduction caused by the lower Q-value needed to accommodate pulses at ω_A and ω_B. A bimodal resonator lets mw pulses at ω_A and ω_B be placed at the center of their own mode, which allows both modes to have better Q-values, for even greater B_1 fields, Fig. 2.7b.

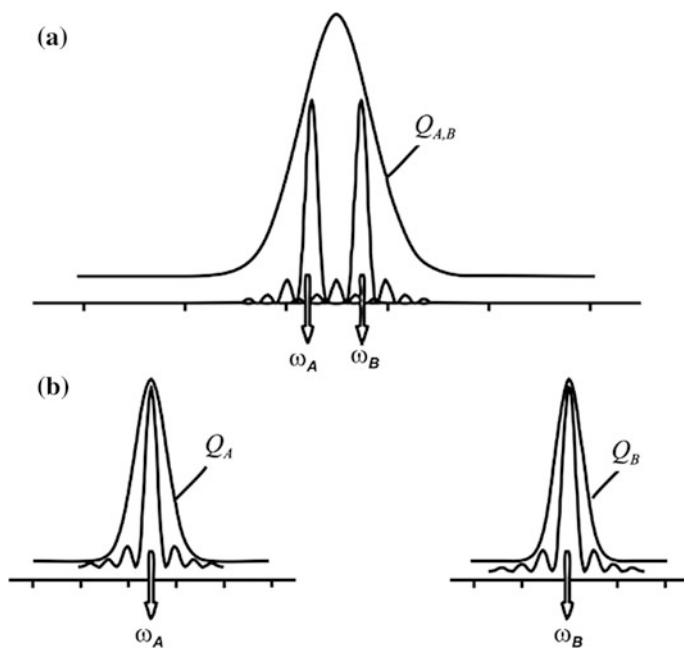**Fig. 2.7** Locations of observe pulses at ω_A and the pump pulses at ω_B, relative to the resonance curve for **a** a single-mode and **b** a bimodal resonator [30]

2.6.5   Determination of p_B

The EPR spectrum, the desired $\Delta\omega_{AB}$, and the duration of the mw pulses limit choices for ω_A and ω_B in PELDOR. The excitation spectra of the observe and pump pulses should not overlap; i.e., it is necessary that $\Delta\omega_{AB}t_p \gg 1$; but, at the same time, $\Delta\omega_{AB} < \Delta$, where Δ is the effective width of the EPR spectrum. For nitroxyl labels at X-band, $\Delta \sim 300\,\text{MHz}$; an experiment with $\Delta\omega_{AB} \sim 100\,\text{MHz}$ requires $t_p \gtrsim 40\,\text{ns}$, which is easily met. However, there are inherent limitations for PELDOR with narrow EPR spectra or with short pulses.

The parameter p_B in Eq. (2.12) is necessary to analyze the PELDOR time trace. It is related to the rotation angle θ of spins B under the ω_B pulse. If the width of the spectrum of spins B is small compared to the pump pulse B_1, all spins rotate by the same angle and p_B can be defined as

$$p_B = \sin\left(\frac{\theta}{2}\right)^2 = \sin\left(\frac{\gamma B_1 t_p}{2}\right)^2 \qquad (2.12)$$

For a broad EPR spectrum, (2.12) should be averaged over the EPR line shape $g(\omega)$. For a rectangular pulse, p_B can be calculated as [1, 4]:

$$p_B = \int\limits_{-\infty}^{+\infty} \frac{\omega_1^2\, g(\omega)}{\omega_1^2 + (\omega_B - \omega)^2} \frac{\sin\left(\frac{t_p}{2}\sqrt{\omega_1^2 + (\omega_B - \omega)^2}\right)^2}{2\pi}\, d\omega \qquad (2.13)$$

where $\omega_1 = \gamma B_1$. The p_B value can be calculated if the EPR line shape $g(\omega)$ and the pump pulse duration t_p are already known.

Experimental determination of p_B seems more reliable. For example, p_B can be determined from the phase relaxation of a model system with a known concentration of uniformly distributed spins using Eq. 1.17. This can be done with ease for glassy solutions of stable radicals. The p_B value can also be obtained for radical pairs known to have $N = 2$ using Eq. 1.16. Methods to determine p_B can be used to determine p_A.

References

1. Mims WB (1965) Electron echo methods in spin resonance spectrometry. Rev Sci Instrum 36 (10):1472–1479. https://doi.org/10.1063/1.1719359
2. Blumberg WE, Mims WB, Zuckerman D (1973) Electron-spin echo envelope spectrometry. Rev Sci Instrum 44(5):546–555. https://doi.org/10.1063/1.1686179
3. Huisjen M, Hyde JS (1974) Pulsed EPR spectrometer. Rev Sci Instrum 45(5):669–675. https://doi.org/10.1063/1.1686710
4. Salikhov KM, Semenov AG, Tsvetkov YD (1976) Electron spin echo and its applications. Nauka, Novosibirsk

5. Holczer K, Schmalbein D (1987) ESP 380: a high-power, general-purpose pulsed EPR spectrometer. Bruker Report 1(1987):22–25
6. The BRUKER FT EPR Spectrometer ESP 380 (1989). In: Keijzers CP, Reijerse EJ, Schmidt J (eds) Pulsed EPR: a new field of applications. Koninklijke Nederlandse Akademie van Wetenschappen, Amsterdam
7. Schmalbein D, Maresch GG, Kamlowski A, Hofer P (1999) The Bruker high-frequency-EPR system. Appl Magn Reson 16(2):185–205. https://doi.org/10.1007/Bf03161933
8. The new technology X-band microwave bridge for CW- and FT-EPR (2001). Bruker report 149/2001, pp 14–15
9. Smith GM, Cruickshank PAS, Bolton DR, Robertson DA (2008) High-field pulse EPR instrumentation. In: Electron paramagnetic resonance, vol 21. The Royal Society of Chemistry, pp 216–233. https://doi.org/10.1039/b807958g
10. Tkach I, Halbmair K, Hobartner C, Bennati M (2014) High-frequency 263 GHz PELDOR. Appl Magn Reson 45(10):969–979. https://doi.org/10.1007/s00723-014-0581-z
11. Poole CP (1983) Electron spin resonance: a comprehensive treatise on experimental techniques/second edition. John Wiley, New York
12. Bender C, Berliner LJ (eds) (2004) EPR: instrumental methods, vol 21. Biological magnetic resonance. Springer US, New York
13. Bender C (2004) The generation and detection of electron spin echoes. In: Bender C, Berliner LJ (eds) EPR: instrumental methods, vol 21. Springer US, New York, pp 212–276. https://doi.org/10.1007/978-1-4419-8951-2
14. Semenov AG, Shchirov MD, Zhidkov VD, Khmelinskii VE, Dvornikov EV (1980) A coherent electron spin echo spectrometer. Preprint No. 3 of the Institute of Chem. Kinetics and Combustion, Novosibirsk
15. Hoefer P, Carl PJ (2006) X-band pulse-EPR resonator performance. Bruker Report 157 (158):52–56
16. Piasecki W, Froncisz W, Hyde JS (1996) Bimodal loop-gap resonator. Rev Sci Instrum 67 (5):1896–1904
17. Rinard GA, Eaton GR (2005) Loop-Gap resonators. In: Eaton SR, Eaton GR, Berliner LJ (eds) Biomedical EPR, Part B: methodology, instrumentation, and dynamics. Springer US, Boston, MA, pp 19–52. https://doi.org/10.1007/0-306-48533-8_2
18. Raitsimring A, Astashkin A, Enemark JH, Blank A, Twig Y, Song Y, Meade TJ (2012) Dielectric resonator for K_a-band pulsed EPR measurements at cryogenic temperatures: probehead construction and applications. Appl Magn Reson 42(4):441–452. https://doi.org/10.1007/s00723-012-0313-1
19. Hyde JS, Chien JCW, Freed JH (1968) Electron-electron double resonance of free radicals in solution. J Chem Phys 48(9):4211–4226. https://doi.org/10.1063/1.1669760
20. Milov AD, Salikhov KM, Shirov MD (1981) Application of the double resonance method to electron spin echo in a study of the spatial distribution of paramagnetic centers in solids. Sov Phys Solid State 23(4):565–569
21. Milov AD, Maryasov AG, Tsvetkov YD (1998) Pulsed electron double resonance (PELDOR) and its applications in free-radicals research. Appl Magn Reson 15(1):107–143. https://doi.org/10.1007/Bf03161886
22. Tkach I, Sicoli G, Hobartner C, Bennati M (2011) A dual-mode microwave resonator for double electron-electron spin resonance spectroscopy at W-band microwave frequencies. J Magn Reson 209(2):341–346
23. Bowman MK (1990) Fourier Transform Electron Spin Resonance. In: Kevan L, Bowman MK (eds) Modern pulsed and continuous electron spin resonance, vol 1st. Wiley, New York, pp 1–42
24. Mizuta Y, Kohno M, Fujii K (1993) Development of microwave control in pulsed-ESR apparatus. Jpn J Appl Phys 1 32(3a):1262–1267. https://doi.org/10.1143/jjap.32.1262
25. Hoefer P, Kamlowski A (2001) The new technology CW/FT-EPR microwave bridge. pulsed electron-electron double resonance (ELDOR) experiments. Bruker report 149/2001, pp 16–18

26. Hoefer P, Heilig R, Maier DC, Prisecaru I, Schmalbein D (2003) The superQ-FT accessory for pulsed EPR, ENDOR and ELDOR at 34 GHz. Bruker Report 152(153):37–43
27. Carl P, Heilig R, Maier DC, Hoefer P, Schmalbein D (2004) The W-band power upgrade module for pulsed EPR, ENDOR and ELDOR at 94 GHz. Bruker Report 154(155):35–40
28. Borbat PP, Crepeau RH, Freed JH (1997) Multifrequency two-dimensional Fourier transform ESR: An X/Ku-band spectrometer. J Magn Reson 127(2):155–167
29. Goldfarb D, Lipkin Y, Potapov A, Gorodetsky Y, Epel B, Raitsimring AM, Radoul M, Kaminker I (2008) HYSCORE and DEER with an upgraded 95 GHz pulse EPR spectrometer. J Magn Reson 194(1):8–15
30. Tsvetkov YD, Grishin YA (2009) Techniques for EPR spectroscopy of pulsed electron double resonance (PELDOR): a review. Instrum Exp Tech. 52(5):615–636. https://doi.org/10.1134/s0020441209050017
31. Prisner TF, Rohrer M, Mobius K (1994) Pulsed 95-Ghz, high-field EPR heterodyne spectrometer with high spectral and time resolution. Appl Magn Reson 7(2–3):167–183. https://doi.org/10.1007/Bf03162610
32. Dubinskii AA, Grishin YA, Savitsky AN, Mobius K (2002) Submicrosecond field-jump device for pulsed high-field ELDOR. Appl Magn Reson 22(3):369–386. https://doi.org/10.1007/Bf03166118
33. Schnegg A, Dubinskii AA, Fuchs MR, Grishin YA, Kirilina EP, Lubitz W, Plato M, Savitsky A, Mobius K (2007) High-field EPR, ENDOR and ELDOR on bacterial photosynthetic reaction centers. Appl Magn Reson 31(1–2):59–98
34. Rohrer M, Brugmann O, Kinzer B, Prisner TF (2001) High-field/high-frequency EPR spectrometer operating in pulsed and continuous-wave mode at 180 GHz. Appl Magn Reson 21(3–4):257–274. https://doi.org/10.1007/Bf03162406
35. Hertel MM, Denysenkov VP, Bennati M, Prisner TF (2005) Pulsed 180-GHz EPR/ENDOR/PELDOR spectroscopy. Magn Reson Chem 43:S248–S255
36. Denysenkov VP, Prisner TF, Stubbe J, Bennati M (2005) High-frequency 180 GHz PELDOR. Appl Magn Reson 29(2):375–384. https://doi.org/10.1007/Bf03167024
37. Denysenkov VP, Prisner TF, Stubbe J, Bennati M (2006) High-field pulsed electron-electron double resonance spectroscopy to determine the orientation of the tyrosyl radicals in ribonucleotide reductase. P Natl Acad Sci USA 103(36):13386–13390. https://doi.org/10.1073/pnas.0605851103
38. Denysenkov VP, Biglino D, Lubitz W, Prisner TF, Bennati M (2008) Structure of the tyrosyl biradical in mouse R2 ribonucleotide reductase from high-field PELDOR. Angew Chem Int Ed 47(7):1224–1227
39. Biospin B (2017) ELEXSYS E780. https://www.bruker.com/fileadmin/user_upload/8-PDF-Docs/MagneticResonance/EPR_brochures/Elexsys_E780_flyer_0714_T13102_lo-res.pdf. Accessed 14 Mar 2017
40. Rengan SK, Bhagat VR, Sastry VSS, Venkataraman B (1969) Magnetic field-pulsed ELDOR spectroscopy. J Magn Reson 33(2):227–240. https://doi.org/10.1016/0022-2364(79)90242-7
41. Dzuba SA, Tsvetkov YD (1982) Slow rotations of nitroxyl radicals in viscous liquids studied by ESE. Khim Fiz 9:1197–1201
42. Dzuba SA, Maryasov AG, Salikhov KM, Tsvetkov YD (1984) Superslow rotations of nitroxide radicals studied by pulse EPR spectroscopy. J Magn Reson 58(1):95–117
43. Kispert LD (2005) Electron-Electron Double Resonance. In: Eaton SR, Eaton GR, Berliner LJ (eds) Biomedical EPR, Part B: methodology, instrumentation, and dynamics. Springer US, Boston, MA, pp 165–197. https://doi.org/10.1007/0-306-48533-8_6
44. Kulik LV, Grishin YA, Dzuba SA, Grigoryev IA, Klyatskaya SV, Vasilevsky SF, Tsvetkov YD (2002) Electron dipole-dipole ESEEM in field-step ELDOR of nitroxide biradicals. J Magn Reson 157(1):61–68

45. Mobius K, Savitsky A, Schnegg A, Plato M, Fuchs M (2005) High-field EPR spectroscopy applied to biological systems: characterization of molecular switches for electron and ion transfer. Phys Chem Chem Phys 7(1):19–42
46. Davis JL, Mims WB (1981) Use of a microwave delay-line to reduce the dead time in electron-spin echo envelope spectroscopy. Rev Sci Instrum 52(1):131–132. https://doi.org/10.1063/1.1136423
47. Narayana PA, Massoth RJ, Kevan L (1982) Active microwave delay-line for reducing the dead time in electron-spin echo spectrometry. Rev Sci Instrum 53(5):624–626. https://doi.org/10.1063/1.1137021
48. Cho H, Pfenninger S, Gemperle C, Schweiger A, Ernst RR (1989) Zero deadtime pulsed ESR by remote echo detection. Chem Phys Lett 160(4):391–395. https://doi.org/10.1016/0009-2614(89)87616-X
49. Doan PE, Hoffman BM (1997) Making hyperfine selection in Mims ENDOR independent of deadtime. Chem Phys Lett 269(3–4):208–214
50. Pfenninger S, Forrer J, Schweiger A, Weiland T (1988) Bridged loop gap resonator—a resonant structure for pulsed electron-spin-resonance transparent to high-frequency radiation. Rev Sci Instrum 59(5):752–760. https://doi.org/10.1063/1.1139822
51. Fauth JM, Schweiger A, Ernst RR (1989) Recovery of broad hyperfine lines in electron spin-echo envelope modulation spectroscopy of disordered-systems. J Magn Reson 81(2):262–274. https://doi.org/10.1016/0022-2364(89)90058-9
52. Volino F, Csakvary F, Servozga P (1968) Resonant helices and their application to magnetic resonance. Rev Sci Instrum 39(11):1660–1665. https://doi.org/10.1063/1.1683198
53. Mehring M, Freysoldt F (1980) A slotted tube resonator Str for pulsed electron-spin-resonance and odmr experiments. J Phys E: Sci Instrum 13(8):894–895. https://doi.org/10.1088/0022-3735/13/8/022
54. Hyde JS, Froncisz W (1989) Loop gap resonators. In: Advanced EPR. Elsevier, Amsterdam, pp 277–305. https://doi.org/10.1016/b978-0-444-88050-5.50012-4
55. Webb RH (1962) Use of traveling wave helices in ESR and double resonance spectrometers. Rev Sci Instrum 33(7):732–737. https://doi.org/10.1063/1.1717946
56. Biehl R (1986) Sensitivity enhancement in EPR. The dielectric ring TE 011 cavity. Bruker report 1/1986, pp 45–47
57. Ivanov MY, Nadolinny VA, Bagryanskaya EG, Grishin YA, Fedin MV, Veber SL (2016) Bismuth germanate as a perspective material for dielectric resonators in EPR spectroscopy. J Magn Reson 271(Supplement C):83–89. https://doi.org/10.1016/j.jmr.2016.08.009
58. Pfenninger S, Froncisz W, Forrer J, Luglio J, Hyde JS (1995) General-method for adjusting the quality factor of EPR resonators. Rev Sci Instrum 66(10):4857–4865
59. Schweiger A, Jeschke G (2001) Principles of pulse electron paramagnetic resonance. Oxford University Press, Oxford, UK, New York
60. Rinard GA, Quine RW, Eaton SS, Eaton GR (2004) Frequency dependence of EPR sensitivity. In: Berliner LJ, Bender CJ (eds) EPR: instrumental methods. Springer US, Boston, MA, pp 115–154. https://doi.org/10.1007/978-1-4419-8951-2_3
61. Romanelli M, Kurshev V, Kevan L (1994) Comparative-analysis of pulsed electron-spin-resonance spectrometers at X-band and S-band. Appl Magn Reson 7(2–3):427–441. https://doi.org/10.1007/Bf03162623
62. Davoust CE, Doan PE, Hoffman BM (1996) Q-band pulsed electron spin-echo spectrometer and its application to ENDOR and ESEEM. J Magn Reson Ser A 119(1):38–44
63. Salikhov KM, Tsvetkov YD (1979) Electron spin echo studies of spin-spin interactions in solids. In: Kevan L, Schwartz RN (eds) Time domain electron spin resonance. John Wiley, New York, pp 231–278

64. El Mkami H, Ward R, Bowman A, Owen-Hughes T, Norman DG (2014) The spatial effect of protein deuteration on nitroxide spin-label relaxation: Implications for EPR distance measurement. J Magn Reson 248:36–41. https://doi.org/10.1016/j.jmr.2014.09.010

65. Ward R, Bowman A, Sozudogru E, El-Mkami H, Owen-Hughes T, Norman DG (2010) EPR distance measurements in deuterated proteins. J Magn Reson 207(1):164–167. https://doi.org/10.1016/j.jmr.2010.08.002

66. Jeschke G, Bender A, Paulsen H, Zimmermann H, Godt A (2004) Sensitivity enhancement in pulse EPR distance measurements. J Magn Reson 169(1):1–12

67. Ghimire H, McCarrick RM, Budil DE, Lorigan GA (2009) Significantly improved sensitivity of Q-band PELDOR/DEER experiments relative to X-band is observed in measuring the intercoil distance of a leucine zipper motif peptide (GCN4-LZ). Biochemistry-Us 48 (25):5782–5784

68. Zou P, Mchaourab HS (2010) Increased sensitivity and extended range of distance measurements in spin-labeled membrane proteins: Q-band double electron-electron resonance and nanoscale bilayers. Biophys J 98(6):L18–L20. https://doi.org/10.1016/j.bpj.2009.12.4193

69. Swanson MA, Kathirvelu V, Majtan T, Frerman FE, Eaton GR, Eaton SS (2011) Electron transfer flavoprotein domain II orientation monitored using double electron-electron resonance between an enzymatically reduced, native FAD cofactor, and spin labels. Protein Sci 20(3):610–620. https://doi.org/10.1002/pro.595

70. Di Valentin M, Albertini M, Zurlo E, Gobbo M, Carbonera D (2014) Porphyrin triplet state as a potential spin label for nanometer distance measurements by PELDOR spectroscopy. J Am Chem Soc 136(18):6582–6585. https://doi.org/10.1021/ja502615n

71. Kandrashkin YE, van der Est A (2011) Stimulated electron spin polarization in strongly coupled triplet-doublet spin pairs. Appl Magn Reson 40(2):189–204. https://doi.org/10.1007/s00723-011-0194-8

72. Shevelev GY, Krumkacheva OA, Lomzov AA, Kuzhelev AA, Trukhin DV, Rogozhnikova OY, Tormyshev VM, Pyshnyi DV, Fedin MV, Bagryanskaya EG (2015) Triarylmethyl Labels: toward improving the accuracy of EPR nanoscale distance measurements in DNAs. J Phys Chem B 119(43):13641–13648

73. Goldfarb D (2014) Gd^{3+} spin labeling for distance measurements by pulse EPR spectroscopy. Phys Chem Chem Phys 16(21):9685–9699. https://doi.org/10.1039/c3cp53822b

74. Shevelev GY, Lomzov AA, Pyshnyi DV, Kuzhelev AA, Krumkacheva OA, Fedin MV, Rogozhnikova OY, Trukhin DV, Troitskaya TI, Tormyshev VM, Bagryanskaya EG (2015) Spin-labeled oligonucleotides—useful tool for the structural biology. FEBS J 282:350

75. Shevelev GY, Krumkacheva OA, Lomzov AA, Kuzhelev AA, Rogozhnikova OY, Trukhin DV, Troitskaya TI, Tormyshev VM, Fedin MV, Pyshnyi DV, Bagryanskaya EG (2014) Physiological-temperature distance measurement in nucleic acid using triarylmethyl-based spin labels and pulsed dipolar EPR spectroscopy. J Am Chem Soc 136 (28):9874–9877

76. Bagryanskaya EG, Krumkacheva OA, Fedin MV, Marque SRA (2015) Development and application of spin traps, spin probes, and spin labels. Methods Enzymol 563:365–396

77. Kaminker I, Tkach I, Manukovsky N, Huber T, Yagi H, Otting G, Bennati M, Goldfarb D (2013) W-band orientation selective DEER measurements on a Gd^{3+}/nitroxide mixed-labeled protein dimer with a dual mode cavity. J Magn Reson 227:66–71

78. Lovett JE, Lovett BW, Harmer J (2012) DEER-stitch: combining three- and four-pulse DEER measurements for high sensitivity, deadtime free data. J Magn Reson 223:98–106

79. Salvadori E, Fung MW, Hoffmann M, Anderson HL, Kay CW (2015) Exploiting the symmetry of the resonator mode to enhance PELDOR sensitivity. Appl Magn Reson 46 (4):359–368. https://doi.org/10.1007/s00723-014-0621-8

80. Srivastava M, Anderson CL, Freed JH (2016) A new wavelet denoising method for selecting decomposition levels and noise thresholds. IEEE Access 4:3862–3877. https://doi.org/10.1109/ACCESS.2016.2587581
81. Srivastava M, Georgieva ER, Freed JH (2017) A new wavelet denoising method for experimental time-domain signals: pulsed dipolar electron spin resonance. J Phys Chem A 121(12):2452–2465. https://doi.org/10.1021/acs.jpca.7b00183
82. Daubechies I (1992) Ten lectures on wavelets. CBMS-NSF regional conference series in applied mathematics. Society for industrial and applied mathematics. https://doi.org/10.1137/1.9781611970104
83. Mailer C, Haas DA, Hustedt EJ, Gladden JG, Robinson BH (1991) Low-power electron-paramagnetic resonance spin-echo spectroscopy. J Magn Reson 91(3):475–496. https://doi.org/10.1016/0022-2364(91)90375-4
84. Blok H, Akimoto I, Milikisyants S, Gast P, Groenen EJJ, Schmidt J (2009) FID detection of EPR and ENDOR spectra at high microwave frequencies. J Magn Reson 201(1):57–60. https://doi.org/10.1016/j.jmr.2009.08.002